

# A detailed dynamic parameter identification procedure for quasi-dynamic testing of solar thermal collectors

J.M. Rodríguez-Muñoz, I. Bove and R. Alonso-Suárez

Laboratorio de Energía Solar, Universidad de la República (Uruguay)

## Abstract

There are two procedures for parameter identification in the standard quasi-dynamic testing of solar thermal collectors: multilinear regression (MLR) and dynamic parameter identification (DPI). The main advantage of DPI is that it is more flexible with respect to the collector model, allowing the use of more sophisticated thermal models and the reduction of testing time. However, most of the implementations available in the literature require non-free close source software, making its replication a difficult task for most testing laboratories. In this work we show a specific implementation of a dynamic parameter identification procedure for a flat plate collector. The algorithm is described in detail, and we also provided a free open-source code in Matlab, facilitating the reproduction of our work and attempting to extend the use of this procedure. We validated its implementations against the standard MLR, comparing the model parameter's values, the efficiency curve and the useful power produced by the collector under the Reporting Standard Conditions defined by the ISO 9806 standard. The measurements were taken in local test facility that compliant with the ISO 9806:2017 requirements.

*Keywords: Solar thermal collectors, parameter identification, quasi-dynamic testing, ISO 9806.*

---

## 1. Introduction

The ISO 9806 (2017) is the most used standard to characterize the thermal performance of solar collectors. It establishes a general thermal model that can be used for a wide variety of technologies: uncovered collectors, flat plate, vacuum tubes, concentrating collectors, etc. This standard admits two test methodologies: Steady State Testing (SST) and Quasi-Dynamic Testing (QDT). For the latter, the determination of the models' parameters (parameter identification) can be done in two different ways. The first one consists in approximating the time derivative by using finite differences and treating it like an independent variable for a multi-linear regression (MLR), which is the most used tool. The second one consists in performing a dynamic simulation coupled with a nonlinear regression algorithm (Dynamic Parameter Identification, DPI). Fischer et al. (2003) showed the equivalence between these two procedures for four different flat plate collectors.

The MLR procedure requires the model to be linear with respect to its parameters, which imposes important limitations on the collector modeling. The DPI procedure is more flexible than MLR with respect to the form that the collector's model can take, allowing the use of more sophisticated thermal models. For instance, it allows the use multi-nodes models, which have been proven to be suitable for in-situ testing, as they are capable of handling large variations in the fluid temperature at the inlet of the collector (Muschaweck & Spirkel, 1993; Fhar et al., 2018). DPI also admits the use of low temporal resolution test data, 10-seconds for example, as shown in Hoffer et al. (2015). The combination of multi-nodes models and low temporal resolution test data allows to better reproduce the real dynamics of the collector, improving the modeling of the transient phenomena and resulting in shorter testing times (Hoffer et al., 2015). Finally, DPI makes it easier to incorporate non-linear incident angle modifier, like the Ambrosetti function for flat plate collectors (Bosanac et al., 1994; J.M. Rodríguez-Muñoz et al., 2021a) or the biaxial incident angle modifiers of tubular collectors. However, the DPI procedure has the disadvantage that its implementation requires the use of more complex mathematical tools. Some implementations of this procedure are described in the literature, but they are based on the use of closed code or paid programs, which makes their replication difficult (Muschaweck & Spirkel,

1993; Hoffer et al., 2015).

In this work we describe in detail a specific implementation of a DPI procedure for a flat plate collector. The algorithm is implemented for this type of collector, and it is validated against the standard MLR procedure, comparing the model parameter's values, the efficiency curve and the useful power produced by the collector under the Reporting Standard Conditions defined by the ISO 9806 standard. A free and explained code in Matlab is also provided, facilitating the reproduction of our work and attempting to extend the use of this procedure into other testing laboratories. The availability of such free and open algorithms represents an important basis for future research in the field of solar collector testing. It will allow the evaluation of different solar collector models with the aim of improving the description of the transient behavior in solar collectors and the reduction of testing times, which is part of our current work.

This article is organized in the following way. Section 2 describes both parameter identification procedures MLR and DPI. Section 3 describes the test facility and the test data used for this work and Section 4 presents the results. Finally, Section 5 summarizes our conclusions.

## 2. Description of parameter identification procedures

### 2.1 Thermal model

The ISO 9806:2017 standard proposes a general thermal model that can be applied to different kinds of solar thermal collectors' technologies. Depending on the collector type, some terms and coefficients can be neglected in the general model. Eq. 1 shows the thermal model for low temperature collectors with cover.

$$\frac{\dot{Q}_u}{A_G} = \eta_{0,b} \cdot [K_b(\theta) \cdot G_b + K_d \cdot G_d] - a_1(T_m - T_a) - a_2(T_m - T_a)^2 - a_5 \frac{dT_m}{dt} \quad (\text{eq. 1})$$

where  $G_b$  and  $G_d$  are the direct and diffuse solar irradiance on the collector plane, respectively,  $T_m$  is the mean temperature of the working fluid (the average between the inlet temperature,  $T_i$ , and the outlet temperature,  $T_o$ ),  $T_a$  is the temperature of the surrounding air, and the characteristic parameters are:  $\eta_{0,b}$ ,  $K_b(\theta)$ ,  $K_d$ ,  $a_1$ ,  $a_2$  y  $a_5$ . The first three parameters are related with the optic efficiency,  $a_1$  and  $a_2$  are the heat loss factor parameters (where the  $a_2$  coefficient is needed for modeling the non-linear radiative losses) and  $a_5$  is the effective thermal capacity divided by the gross collector area ( $A_G$ ). All these parameters are assumed to be constants (since the test is carried out at constant flow rate) except for the incident angle modifier for the direct solar irradiance,  $K_b(\theta)$ . For this last parameter, the expression of eq. 2 can be used, where  $\theta$  is the angle of incident (Souka & Safwat, 1966).

$$K_b(\theta) = 1 - b_0 \left( \frac{1}{\cos(\theta)} - 1 \right) \quad (\text{eq. 2})$$

### 2.2 Multilinear regression algorithm

The application of the MLR algorithm requires the definition of the dependent variable, in this case, the useful power produced by the collector per unit of gross area, and the definition of the independent variables, in this case:  $G_b$ ,  $(1/\cos(\theta)-1) G_b$ ,  $G_d$ ,  $(T_m-T_a)$ ,  $(T_m-T_a)^2$  y  $dT_m/dt$ . The last variable is approximate by finite difference using the measured data. Then, the characteristic parameters are determined by the following equation, which is a standard multivariate least mean squares algorithm:

$$p = (X^T X)^{-1} X^T y \quad (\text{eq. 3})$$

In this equation  $p$  is a vector containing the parameters' values,  $X$  is a matrix with the independent variables as columns and  $y$  the dependent variable. The uncertainty for each parameter is derived from the covariance matrix, whose detailed calculation can be consulted in Kratzenberg et al. (2006).

### 2.3 Dynamic parameter identification algorithm

The DPI procedure implemented in this work is summarized in Fig. 1. This is an iterative procedure that begins with an initial guess of the parameters' vector  $p$  (a seed), and uses the measured data, the thermal model given by eq. (1) and a cost function to determine an optimal value of  $p$  within a certain tolerance. Each part of this algorithm is described separately below.

The first step is the definition of a cost function. In the field of solar collector testing, a proper cost function is

the mean square error of the useful power estimation,

$$E_c(p) = \frac{1}{M} \sum_{i=1}^M [\dot{Q}_u - \dot{Q}_u^*(p)] \quad (\text{eq. 4})$$

where M is the number of measurement and the superscript \* indicates that the variable corresponds to a theoretical model's estimate. This nomenclature is introduced with the aim of facilitating the differentiate between model's estimate ( $\dot{Q}_u^*, T_m^*$ ) and the measured data ( $\dot{Q}_u, T_m$ ). It is noted that the cost function depends on the vector of parameters  $p$ .

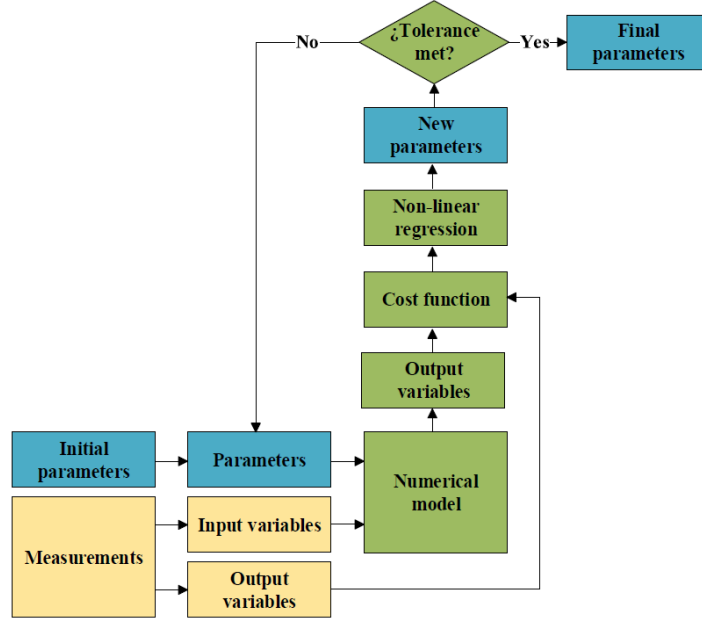


Fig. 1: Illustration of the dynamic parameter identification procedure.

The second step is the implementation of a numerical method to solve the differential equation given by eq. (1). The output variables ( $\dot{Q}_u^*, T_m^*$ ) are obtained based on the input variables and a set of characteristic parameters  $p$ . The input variables correspond to measurements of relevant variables in collector modeling, such as  $T_i(t)$ ,  $T_a(t)$ ,  $m(t)$ ,  $G_b(t)$  and  $G_d(t)$ , which are static functions of time in each iteration. The characteristic parameters of the collector vary in each iteration. For convenience, eqs. (1) and (2) are rewritten as follows,

$$\frac{dT_m^*}{dt} = F(t, T_m^*) \quad \text{with}$$

$$F(t, T_m^*) = \frac{1}{a_5} \left[ \eta_{0,b} \cdot \left( 1 - b_0 \left( \frac{1}{\cos(\theta)} - 1 \right) \right) \cdot G_b + \eta_{0,b} \cdot K_d \cdot G_d - a_1(T_m^* - T_a) - a_2(T_m^* - T_a)^2 - \frac{2\dot{m}c_p(T_m^* - T_i)}{A_G} \right] \quad (\text{eq. 5})$$

Assuming that the value of  $T_m^*$  at the initial time,  $t_0$ , is known, the value of  $T_m^*$  at a generic time  $t_i$ , that is,  $T_m^*(t_i)$ , is determined by integrating eq. (5) between the instants  $t_i$  and  $t_{i-1}$ . This integral is performed using the trapezoid methods, i.e., the area under the curve is approximated by the area of a trapezoid as follows:

$$T_m^*(t_i) = T_m^*(t_{i-1}) + \frac{\Delta t}{2} [F(t_i, T_m^*(t_i)) + F(t_{i-1}, T_m^*(t_{i-1}))] \quad (\text{eq. 6})$$

This equation is not linear with respect to  $T_m^*$ , and can be solved, for each instant, by means of a fixed-point iteration. As an initial value to begin this iteration, the solution is joined with the forward Euler method.

$$T_m^*(t_i) = T_m^*(t_{i-1}) + \Delta t F(t_i, T_m^*(t_i)) \quad (\text{eq. 7})$$

The trapezoid method was chosen for its simplicity; however, other integration methods were implemented but no significant differences in results were obtained.

Then, the theoretical estimate of useful power can be calculated as follow,

$$\dot{Q}_u^* = 2\dot{m}c_p(T_m^* - T_i) \quad (\text{eq. 8})$$

The final step is the implementation of a non-linear regression algorithm. This algorithm will find the optimal vector of parameter  $\hat{p}$  minimizing the cost function. Many algorithms are available in the literature. In this work a Gauss-Newton algorithm was used (Quarteroni, 2000), which consist of linearizing the function  $\dot{Q}_u^*(p)$  around a working point  $p_0$ , that is,

$$\dot{Q}_u^*(p) \approx \dot{Q}_u^*(p_0) + J(p_0)(p - p_0) \quad (\text{eq. 9})$$

were  $J(p_0)$  is the Jacobian matrix of the function  $\dot{Q}_u^*(p)$  evaluated in the working point  $p_0$ . The entries of this matrix are numerically estimated using central finite difference as follow,

$$J(p_0)_{i,j} = \frac{\dot{Q}_u^*(t_i, p_0 + \delta p_j) - \dot{Q}_u^*(t_i, p_0 - \delta p_j)}{2\delta p_j} \quad (\text{eq. 10})$$

For  $\delta p_j$  the value suggested by Bates and Watts (1988) was used, that is,  $\delta p_j = \varepsilon p_0$ , where  $\varepsilon$  is the epsilon machine. Then, the solution of the linearized sample can be found in the same way as in the linear case. In this sense, the optimal set of parameters,  $\hat{p}$ , that minimizes the cost function around the working point is:

$$\hat{p} = p_0 + (J(p_0)^T J(p_0))^{-1} J(p_0)^T [\dot{Q}_u - \dot{Q}_u^*(p_0)] \quad (\text{eq.11})$$

This procedure is iterative, it starts with an initial seed  $p_0$  and calculates  $\dot{Q}_u^*(p_0)$  y  $J(p_0)$ ; then  $\hat{p}$  is determined with eq. (11) and the process restart with  $p_0 = \hat{p}$ . The process continues until the difference between  $p_0$  and  $\hat{p}$  is less than a certain tolerance. One drawback of this method is that the solution can converge to a local minimum and not to the global minimum, for this reason, the process is repeated using 10 different randomly generated initial seeds. If the algorithm converges to different solutions, then the solution with the smallest mean square error (global minimum) is chosen. The estimation of the uncertainty of the parameters in this case can be done in the same way as in the linear case, replacing the matrix  $X$  by the matrix  $J(\hat{p})$ . A script in Matlab that allows to calculate the model's parameters and its uncertainty is provided in [http://les.edu.uy/RDpub/RBA\\_DPI\\_tool.zip](http://les.edu.uy/RDpub/RBA_DPI_tool.zip)

### 3. Tests facilities and data

#### 3.1 Test facilities

The measurements were taken at the Solar Heaters Test Platform (BECS) of the Solar Energy Laboratory (LES, <http://les.edu.uy/>) of the Universidad de la República (UdelaR), which is located near the city of Salto (Latitude=31.28°S, Longitude=57.92°W), Uruguay. Recently, the BECS participated in a Latin American inter-comparison of test laboratories organized by the PTB (Physikalisch-Technische Bundesanstalt), the German Metrological Institute, an activity in which the platform obtained the best qualification for almost all tests and just one minor observation in the determination of a secondary variable (Fischer, 2020).



Fig. 2. Test bench.

Fig. 2 show a photo of the test bench. To measure the temperature at the input and output of the collector a 3 wire PT100 with 4-20 mA transmitters from Herten company were used. These sensors were calibrated at LES using a calibrated thermal bath and calibrated reference thermometers, reporting a standard uncertainty (P67,  $k = 1$ ) of 0.02 °C. Ambient temperature was recorded with a Honeywell 2-wire PT1000 sensor also calibrated at LES with a standard uncertainty of 0.02 °C. The flow measurement was performed with an Endress & Hauser electromagnetic flowmeter with a standard uncertainty of 0.5 % of the measurement. The wind speed parallel to the collector plane was measured with an NGR cup anemometer with a standard uncertainty of 0.25 m/s. The global irradiance in the collector plane was measured with a Kipp & Zonen CMP10 pyranometer. The global irradiance in the horizontal plane ( $G_h$ ) was measured with a Kipp & Zonen CMP11 pyranometer and the diffuse irradiance in the horizontal plane ( $G_{dh}$ ) with a Kipp & Zonen CMP6 pyranometer mounted with a shadow band from the same manufacturer. All the pyranometers used are spectrally flat (ISO-9060, 2018), being Class A for the global irradiance measurements and Class B for the diffuse irradiance measurement. The diffuse irradiance measurement (with shadow band) was corrected with the expression provided by the manufacturer (Drummond, 1956). These pyranometers are calibrated annually at the LES according to the ISO-9847 (1992) standard against a Kipp & Zonen CMP22 secondary standard that is kept traceable to the world radiometric reference at the World Radiation Center in Davos, Switzerland. All measurements were recorded every 10 seconds using a Fischer Scientific DT85 datalogger. The direct irradiance in the collector plane  $G_b$  was estimated from the  $G_h$  and  $G_{dh}$  with the following procedure. First, the direct normal irradiance (DNI) was calculated using the closure relation  $G_h = \text{DNI} \cos \theta_z + G_{dh}$ , where  $\cos \theta_z$  is the cosine of the solar zenith angle. Then, the  $G_b$  was calculated from the DNI, by multiplying with the cosine of the incident angle. A flat plate solar thermal collector with a gross area of 2.02 m<sup>2</sup> was used for this work, which was the reference collector also used in the aforementioned inter-comparison of test laboratories. The hydraulic installation of the BECS is described in detail in Rodríguez-Muñoz et al. (2021a).

### 3.2 Data

The tests were performed according to the ISO-9806 (2017) standard. During the tests, a wind speed of 3 m/s (spatial average) was imposed along the collector plane by using the air forcings shown in Fig. 2. The fluid flow was set at 2.4 l/min and the tracker inclination angle was set at 45°. The azimuth was adjusted manually or automatically depending on the day type. The day types correspond to specific test sequences defined by the ISO-9806 (2017) standard and there are 4 different day types in total. Each of these sequences (day type) must have a duration of at least 3 hours and may be made up of several non-consecutive subsequences of at least 30 minutes each. The procedure and the purpose of each day type is described in the standard.

Fig. 3 shows the graphs suggested by the standard to assess the variability of the operating conditions of the measurement set, where each data (blue point) corresponds to an average of 5 minutes. In Fig. 3a, clear sky and cloudy conditions can be distinguished, the values that follow a regularity are those associated with clear skies. The red line with slope 1 ( $G = G_d$ ) in this figure is used to perform a basic quality control; the  $G_d$  and  $G_t$  measurements must be below the red line because  $G_d < G$ . Fig. 3b shows the different inlet temperatures, and Fig. 3c shows the variability in the incidence angle. In this last graph, the negative and positive values correspond to measurements made before and after solar noon, respectively.

A total of 6780 measurement samples were registered, at a 10 seconds time rate. The data must be averaged every certain period prior to the parameter's identification, a time that is not specified in the standard. Different averaging times were tried between 30 seconds and 10 minutes for the MRL method. We found that the parameters' value does not change significantly except for the one associated with the thermal capacity,  $a_s$ , which tends to a constant value and close to the value obtained with the SST method from an averaging time of 5 minutes. Also, the parameters' uncertainty tends to grow with averaging time. For this reason, we chose a 5-minute averaging time for the MLR method, time that coincides with that used in other publications for this same type of collector (Fisher et al., 2003; Fhar et al., 2018). This study was replicated for the DPI method and was found that the time averaging of 30 seconds is the best for this method. The full study of the effect of time averaging on the results can be found in Rodríguez-Muñoz et al. (2021b).

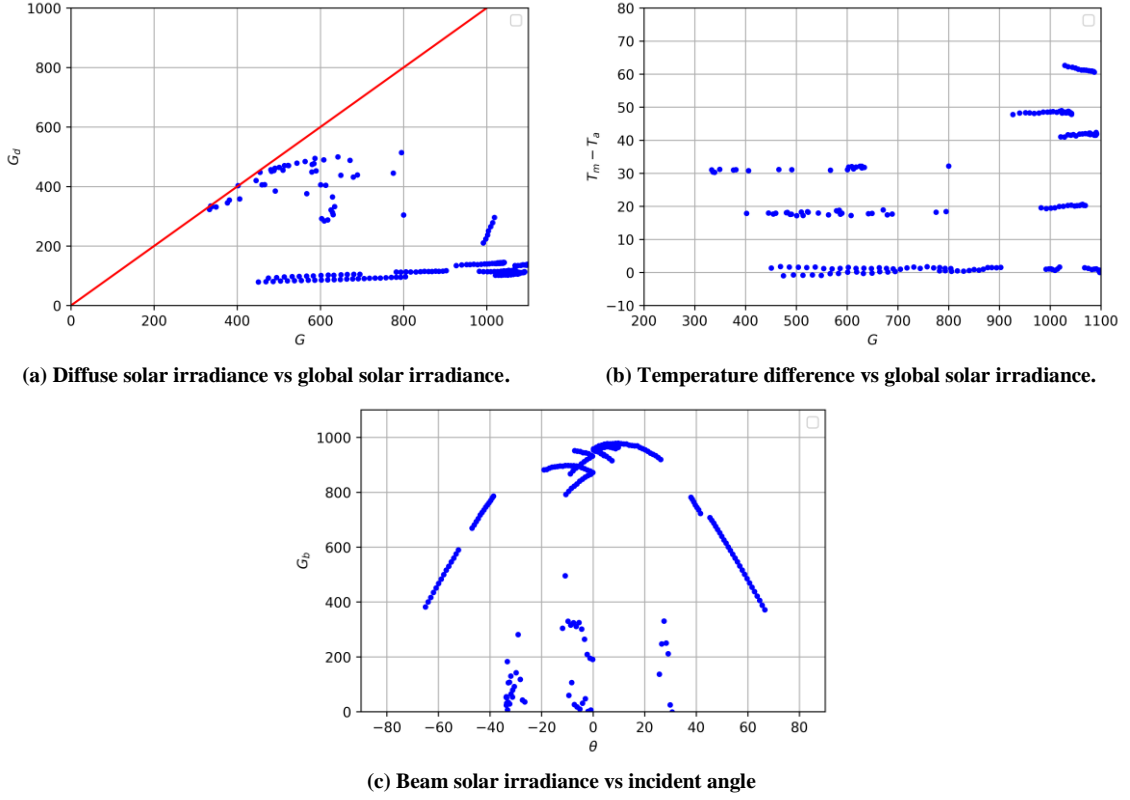


Fig 3. Data set used for the parameter identification.

## 4. Results

The characteristic parameters were identified with the two described procedures. Tab. 1 shows the obtained values, uncertainties, and t-ratios (quotient between the value of the parameter and its uncertainty). The parameters' values are similar for both procedures. The higher difference is 14 % and corresponds to the  $a_2$  parameter. In the rest the differences are less than 2 %. However, the best way to compare the thermal loss factors is through a global positive loss factor:  $a = a_1 + a_2 (T_m - T_a)$ . If a temperature difference of 50 K is considered, the global loss factor is 4.669 W/m<sup>2</sup>.K for the MLR and 4.667 W/m<sup>2</sup>.K for the DPI, being the difference less than 0.1 %. Complementing this information, Fig. 4 shows the efficiency curve for each case (MLR and DPI) for clear sky conditions, that is,  $G_b = 850$  W/m<sup>2</sup> and  $G_d = 150$  W/m<sup>2</sup>, and the 95 % confident interval using the MLR results (black dot line). This figure shows the excellent agreement between both procedures for the entire temperature range, despite the large difference in second order loss factor  $a_2$ .

Tab. 1: Value, uncertainty and t-ratio of the characteristic parameters of each parameter identification procedure.

Parameter	MLR			DPI		
	Value	Uncertainty	t-ratio.	Value	Uncertainty	t-ratio.
$\eta_{0,b}$	0.724	0.001	724	0.725	0.001	725
$b_0$	0.120	0.005	24	0.121	0.001	121
$K_d$	0.970	0.006	162	0.967	0.002	483
$a_1$ (W/m <sup>2</sup> .K)	4.244	0.114	37	4.172	0.029	143
$a_2$ (W/m <sup>2</sup> .K <sup>2</sup> )	0.0085	0.0020	4.3	0.0099	0.0005	20
$a_5$ (J/K.m <sup>2</sup> )	11020	565	20	11126	100	111

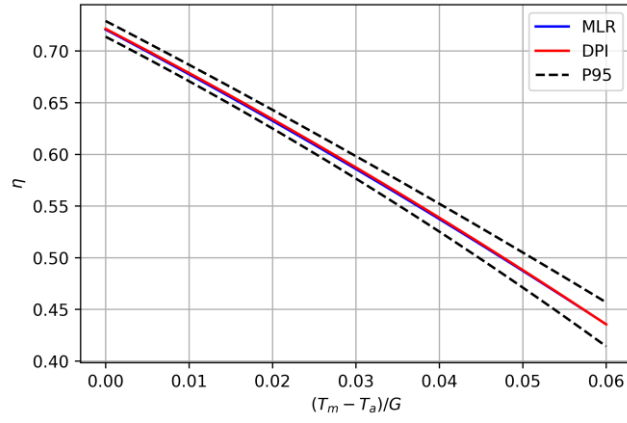
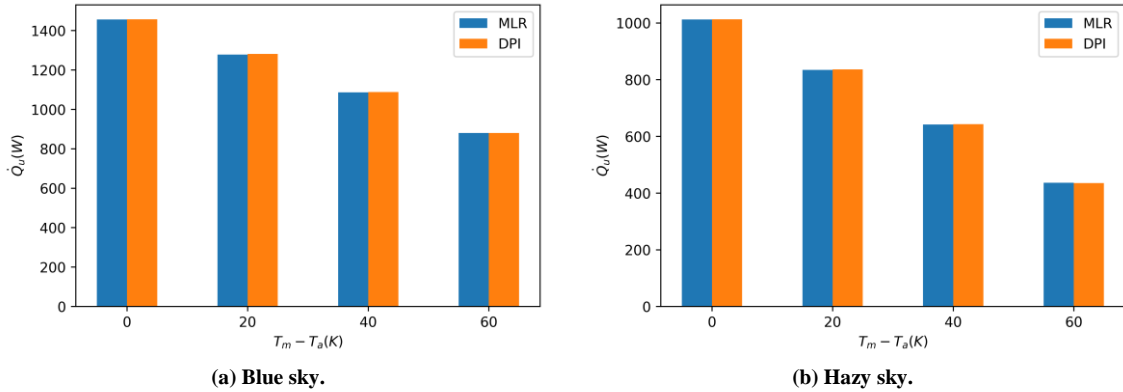


Fig 4. Efficiency curve for each parameter identification procedure.

Finally, to study the combined effect of the differences between the parameters, the useful energy produced by the collector was calculated for each case using eq. (1), assuming normal incidence and steady state, for different temperature and sky conditions. For the different sky conditions, the standard reporting Standard Reporting Conditions (SRC) given by the ISO 9806: 2017 standard were used, and results are show in Tab. 2 and Fig. 5. It can be seen that the difference in useful power is less than 0.2 % for all cases, that is, for all sky conditions and temperature differences.

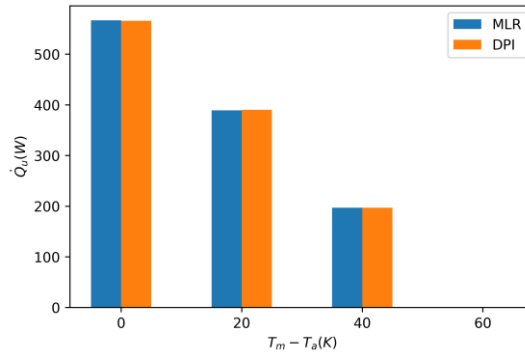
Tab. 2: Useful power (W) produced by the collector for SRC.

$(T_m - T_a)$	Blue sky ( $G_b = 850 \text{ W/m}^2$ , $G_d = 150 \text{ W/m}^2$ )			Hazy sky ( $G_b = 440 \text{ W/m}^2$ , $G_d = 260 \text{ W/m}^2$ )			Grey sky ( $G_b = 0 \text{ W/m}^2$ , $G_d = 400 \text{ W/m}^2$ )		
	MLR	DPI	Dif.	MLR	DPI	Dif.	MLR	DPI	Dif.
0	1456	1457	0.1 %	1012	1013	0.0 %	567	566	-0.2 %
20	1278	1281	0.2 %	834	836	0.2 %	389	390	0.2 %
40	1086	1088	0.2 %	642	643	0.2 %	197	197	0.2 %
60	880	880	0.0 %	436	435	0.3 %	0	0	n.a.



(a) Blue sky.

(b) Hazy sky.



(c) Grey sky.

Fig 5. Useful power (W) produced by the collector for SRC.

## 5. Conclusions

In this work we describe a specific implementation of a DPI procedure for the standardized quasi-dynamic testing of flat plate solar thermal collectors. This implementation was successfully validated against the standard MLR procedure. A complete description of the procedure and a freely accessible and explained code in Matlab was given in this paper, encouraging the use of this algorithm. The development of such a free and open algorithm represents an important basis for future research in the field of solar collector testing. A future work is the implementation of multi-node models and the comparison of their performance against the single-node model of the ISO 9806 (2017), attempting to improve the description of transient phenomena and looking to reduce the duration of the test. Another future work is the extension of the use of this algorithm for other collector technologies, for instance, evacuated solar collector and unglazed collector.

## 6. Acknowledgments

The authors would like to thank the Ministerio de Industria, Energía y Minería (MIEM, Uruguay), especially its Dirección Nacional de Energía (DNE), the Fideicomiso Uruguayo de Ahorro y Eficiencia Energética (Fudae, Uruguay) and the Corporación Nacional para el Desarrollo (CND, Uruguay), for having provided financial and logistical support for the development of the BECS facility and for having promoted this project with local capacities. The authors are also grateful to the PTB of Germany for promoting and financing the inter-laboratory on efficiency test of solar collectors, which has given us technical certainty about our local testing capabilities.

## 7. References

- Bates, D. M. and Watts, D. G. (1988). *Nonlinear regression analysis and its applications*. John Wiley & Sons.
- Bosanac, M., Brunotte, A., Spirkl, W., and Sizmann, R. (1994). The use of parameter identification for flat-plate collector testing under non-stationary conditions. *Renewable Energy*, 4(2):217-222. doi: [https://doi.org/10.1016/0960-1481\(94\)90006-X](https://doi.org/10.1016/0960-1481(94)90006-X)
- Drummond, A. J. (1956). On the measurement of sky radiation. *Archiv fur Meteorologie, Geophysik und Bioklimatologie, Serie B*, 7:413 - 436. doi: [10.1007/BF02242969](https://doi.org/10.1007/BF02242969).
- Fhar, S. Gumbel, U. Zirkel-Hofer, A. and Kramer, K. (2018). In situ characterization of thermal collectors in field installations. *In EuroSun 2018 Conference Proceedings*. doi: <https://doi.org/10.18086/eurosun2018.12.01>.
- Fisher, S., Müller-Steinhagen, H., & Perers, B. (2003). Collector parameter identification - iterative methods versus multiple linear regression. *ISES Solar World Congress*. Presented at the ISES Solar World Congress, Gothenburg, Sweden, 16-19/6, 2003.
- Fisher S. (2020). Expert Report - Quality Infrastructure for Energy Efficiency and Renewable Energy in Latin America and the Caribbean. + Report #95309. Recuperado de [http://les.edu.uy/papers/Expert\\_Report-RR-Test\\_R1.pdf](http://les.edu.uy/papers/Expert_Report-RR-Test_R1.pdf)
- Hofer A., Büchner D., Kramer K., Fahr S., Heimsath A., Platzer W.J., Scholl S. (2015). Comparison of Two Different (Quasi-) Dynamic Testing Methods for the Performance Evaluation of a Linear Fresnel Process eat Collector. *Energy Procedia*, 69: 84-95. doi: <https://doi.org/10.1016/j.egypro.2015.03.011>.
- ISO-9060 (2018). *Solar energy - specification and classification of instruments for measuring hemispherical solar and direct solar radiation*. Standard, International Organization of Standardization, Switzerland.
- ISO-9847 (1992). *Solar energy - calibration of \_eld pyranometers by comparison to a reference pyranometer*. Standard, International Organization of Standardization, Switzerland.
- ISO 9806. (2017). *Solar Energy – Solar thermal collectors – Test methods*. Switzerland: International Organization of Standardization.

- Kratzenberg, M., Beyer, H., and Colle, S. (2006). Uncertainty calculation applied to different regression methods in the quasi-dynamic collector test. *Solar Energy*, 80:1453-1462. doi: <https://doi.org/10.1016/j.solener.2006.03.010>.
- Muschaweck J., Spirkel W. (1993). Dynamic solar collector performance testing. *Solar Energy Materials and Solar Cells*, 30(2):95-105. doi: [https://doi.org/10.1016/0927-0248\(93\)90011-Q](https://doi.org/10.1016/0927-0248(93)90011-Q).
- Quarteroni, A., Sacco, R., and Saleri, F. (2000). *Numerical Mathematics*.
- Rodríguez-Muñoz, J.M., Bove, I., Alonso-Suárez, R. (2021a). Novel incident angle modifier for quasi-dynamic testing of flat plate solar thermal collectors. *Solar Energy*, 224, 112-124. doi: <https://doi.org/10.1016/j.solener.2021.05.026>.
- Rodríguez Muñoz, J. (2021b). *Ensayos de desempeño térmico de colectores solares de placa plana*. Tesis de maestría. Universidad de la República (Uruguay). Facultad de Ingeniería. doi: [10.13140/RG.2.2.23050.18881](https://doi.org/10.13140/RG.2.2.23050.18881).
- Souka, A. and Safwat, H. (1966). Determination of the optimum orientations for the double-exposure, at-plate collector and its reflectors. *Solar Energy*, 10(4):170-174. doi: [https://doi.org/10.1016/0038-092X\(66\)90004-1](https://doi.org/10.1016/0038-092X(66)90004-1).